Dynamics of the Dihydrofolate Reductase−Folate Complex: Catalytic Sites and Regions Known To Undergo Conformational Change Exhibit Diverse Dynamical Features†

David M. Epstein,‡,§ Stephen J. Benkovic,§ and Peter E. Wright*,‡

Department of Molecular Biology, The Scripps Research Institute, 10666 North Torrey Pines Road, La Jolla, California 92037, and Department of Chemistry, 152 Davey Laboratory, The Pennsylvania State University, University Park, Pennsylvania 16802

Received April 12, 1995; Revised Manuscript Received June 2, 1995⊗

ABSTRACT: Backbone and tryptophan side-chain dynamics of uniformly ^{15}N-labeled *Escherichia coli* dihydrofolate reductase were determined for the binary folate complex. The ^{15}N T_1 and T_2 relaxation times and {^{1}H}−^{15}N heteronuclear NOEs were measured for 118 protonated backbone nitrogen atoms. The generalized order parameter (S^2), the effective correlation time for internal motions (τ_e), and the contribution to spin−spin relaxation through ^{15}N exchange broadening (R_{ex}) were determined for each residue by model-free analysis. Back-calculation of the relaxation rates for each resonance showed that the calculated dynamical parameters accurately predict the experimental data. Diverse dynamical features were evident in the DHFR backbone. Six sites exhibited order parameters significantly below the weighted mean S^2 value (for the complex) of 0.81 ± 0.002: residues G67 and D69 of the adenosine binding domain, and "hinge" residues K38 and V88, exhibited low S^2 ($0.29 \leq S^2 \leq 0.6$) and high τ_e values (700 ps $\leq \tau_e \leq$ 2 ns), as did sites within the βA−αB loop and the βF−βG loop. Thus, large amplitude backbone motions, on the picosecond and nanosecond time scales, occurred at regions implicated in transition-state stabilization and in ligand-dependent conformational change. Significant R_{ex} values (≥ 1 s^{-1}) were determined for 45% of assigned resonances, many of which arise from residues surrounding the folate binding site. The mean S^2 values of the occupied folate binding site and the unoccupied NADPH binding site were similar, indicating the backbone of the latter is at least as conformationally restricted as that of the occupied folate site. We conclude that the observed time-dependent structural fluctuations of the binary complex are in fact associated with catalytic properties of the molecule.

Conformational fluctuations in proteins are well documented by kinetic and biophysical methods (Jencks, 1969; Jardetzky & Roberts, 1981; McCammon & Harvey, 1987; Creighton, 1993). Internal motions include dihedral angle fluctuations of the protein backbone (Howarth, 1978; Brüschweiler & Wright, 1994), rotations of amino acid side chains (Wagner et al., 1987), movement of loops (Falzone et al., 1994b), and the relative motions of secondary structure and structural domains (Bennett & Steitz, 1980). It is not yet clear, however, what motional time scales are relevant to enzymic catalysis and which motions affect function? Since a direct correlation has not been demonstrated between dynamics and biochemical activity, the relative contribution of various motions to function is unknown. Recently, however, intriguing insights into protein dynamics and function have been gained through heteronuclear NMR spectroscopy (Barbato et al., 1992; Peng & Wagner, 1992; Akke et al., 1993; Stone et al., 1993; Cheng et al., 1994). We describe herein the use of two-dimensional heteronuclear (^{1}H−^{15}N) nuclear magnetic relaxation to rigorously characterize the backbone dynamics of dihydrofolate reductase (DHFR)[1] in the presence of bound folate. It has been proposed that catalysis in DHFR is affected by internal protein motions (Farnum et al., 1991; Falzone et al., 1994b). The question addressed is whether enzyme sites known to undergo ligand-dependent conformational changes remain flexible even in the presence of bound ligand or whether the enzyme undergoes a rigid, ligand-dependent two-state transition?

^{15}N NMR relaxation analyses may be used to probe enzyme backbone and tryptophan side-chain motions occurring over time scales ranging from picoseconds to milliseconds [reviewed in Palmer (1993); Wagner et al. (1993)]. Model-free analysis (Lipari & Szabo, 1982a,b) provides dynamical information in terms of motional amplitudes [via an order parameter (S^2) reflecting the degree of motional restriction of the NH bond] and motional time scales [via an effective correlation time for internal motions (τ_e) or a ^{15}N exchange broadening (R_{ex}) contribution] for each NH resonance. Values of S^2 and τ_e provide information on

† Supported by National Institutes of Health Grants GM36643 to P.E.W. and GM24129 to S.J.B. D.M.E. is a postdoctoral fellow of the American Cancer Society.

* Corresponding author [phone (619) 554−9721; fax (619) 554−9822].

‡ The Scripps Research Institute.

§ The Pennsylvania State University.

⊗ Abstract published in *Advance ACS Abstracts,* August 1, 1995.

[1] Abbreviations: DHFR, dihydrofolate reductase (5,6,7,8-tetrahydrofolate:NADP$^+$ oxidoreductase, EC 1.5.1.3); MTX, methotrexate; NADPH, nicotinamide adenine dinucleotide phosphate; CPMG, Carr−Purcell−Meiboom−Gill; HSQC, heteronuclear single-quantum correlation; INEPT, insensitive nuclei enhanced by polarization transfer; NMR, nuclear magnetic resonance; NOE, nuclear Overhauser effect; S^2, generalized order parameter, which is a measure of the degree of spatial restriction of the unit bond vector (for the present study, the amide and tryptophan indole NH bonds); T_1, spin−lattice relaxation time constant; T_2, spin−spin or transverse relaxation time constant; TPPI, time-proportional phase incrementation.

0006-2960/95/0434-11037$09.00/0

picosecond to nanosecond time scale motions, whereas R_{ex} provides information on motions in the microsecond to millisecond regime. Since biochemical events such as enzyme turnover rates, ligand binding and dissociation rates, and the rates of conformational change often occur near the time scale of the lower frequency motions, it is plausible that these slower protein motions affect function.

Escherichia coli DHFR (159 residues, 18 kDa) has been characterized in exquisite mechanistic and structural detail. The enzyme utilizes NADPH to reduce 7,8-dihydrofolate (H_2F) to 5,6,7,8-tetrahydrofolate (H_4F). A detailed kinetic scheme is known (Fierke et al., 1987), as are the energetic contributions of active site residues that interact with folate and NADPH [reviewed in Wagner and Benkovic (1990)]. Comparison of DHFR crystal structures, including that of apo-DHFR, the binary complexes with MTX or $NADP^+$, and the DHFR−folate−$NADP^+$ ternary complex reveals subtle ligand-dependent conformational changes (Bolin et al., 1982; Bystroff et al., 1990; Bystroff & Kraut, 1991). In addition, several intriguing dynamical processes are evident in DHFR. Conformational isomerization occurs between two forms of the DHFR−MTX binary complex ($k > 1\ s^{-1}$), as well as between two forms of the apoenzyme (Falzone et al., 1991; Cayley et al., 1981). A critical surface loop (loop 1) covers the active site upon folate binding and fluctuates at a rate of $35\ s^{-1}$ in the apoenzyme; this rate is somehow altered in the folate complex (Falzone et al., 1990; Bystroff & Kraut, 1991; Li et al., 1992; Falzone et al., 1994b). Thus, detailed studies of the ^{15}N dynamics for the DHFR−folate complex are enhanced by the availability of detailed mechanistic and structural information on the enzyme.

MATERIALS AND METHODS

NMR Sample Preparation. ^{15}N-Labeled DHFR was expressed in *E. coli* NCM-533 and purified as previously described (Falzone et al., 1994a). Purified DHFR (0.1 M Tris-HCl, pH 7.0, 2 mM DTE) was stored in a 90% ammonium sulfate pellet at 4 °C. The yield was 25 mg of ^{15}N-DHFR/L of cell culture. A ^{15}N-labeled DHFR-[^{13}C]-C_7,C_9-folate (1:6) complex was prepared by resuspending the ammonium sulfate precipitate (2 mL) and dialyzing twice versus 2 L of 50 mM potassium phosphate, pH 6.8, 1 mM EDTA, and 1 mM DTT at 4 °C. The sample was dialyzed twice versus 1 L of argon-equilibrated (15 min, 22 °C) buffer containing 10 mM potassium phosphate, pH 6.8, and 0.025 mM DTT. The dialysate was lyophilized and then resuspended in argon-equilibrated H_2O (90%), D_2O (10%), 0.1 M KCl, and 1 mM DTT. The final DHFR concentration was determined to be 2 mM, using a molar extinction coefficient of 31 100 $M^{-1}\ cm^{-1}$. Isotopically labeled [^{13}C]-C_7,C_9-folate was prepared by Cowart et al. (1994). ^{15}N-Labeled DHFR and a 6-fold excess of 0.1 M ^{13}C-labeled folate were combined to yield a binary DHFR−folate complex, pH 6.8, 50 mM potassium phosphate, 1 mM [^2H]DTT, and 0.1 M KCl, and the sample was equilibrated under argon. With this excess of folate, we estimate that there is less than 0.5% apo-DHFR in the solution since the K_D of folate is 50 μM (Baccanari et al., 1975, 1977). We used the previously reported ^1H and ^{15}N resonance assignments for the DHFR−folate complex (Falzone et al., 1994a).

NMR Spectroscopy. NMR measurements were performed at 303 K on a Bruker AMX600 spectrometer at ^1H and ^{15}N Larmor frequencies of 600.13 and 60.81 MHz, respectively. Two-dimensional sensitivity-enhanced ^1H-detected heteronuclear NMR spectroscopy was used to measure T_1 and T_2 time constants, and {^1H}−^{15}N steady-state heteronuclear NOEs for protonated ^{15}N nuclei pulse sequences were as described previously (Kordel et al., 1992; Stone et al., 1992; Skelton et al., 1993). Sensitivity-enhanced sequences were used to refocus orthogonal magnetization components following the ^{15}N evolution period (Cavanagh et al., 1991; Palmer et al., 1991, 1992). An auxiliary amplifier (Model 3205, American Microwave Technology) was used to generate high-power ^{15}N pulses for the CPMG sequences in the T_2 experiments. Data were processed using a modified version of FTNMR (Hare Research). Data analyses were performed with in-house FORTRAN programs written by Dr. A. G. Palmer, III.

Model-Free Analysis. Model-free parameters were determined from T_1, T_2, and {^1H}−^{15}N NOE data using the program Modelfree 3.1 (Palmer et al., 1991). Procedures used to find the optimum values and uncertainties, based on the measured relaxation rate constants and NOE values, are similar to those described previously, as are the methods of error analysis and statistical analysis of the data (Palmer et al., 1991; Stone et al., 1993).

The mechanism for relaxation of protonated ^{15}N is primarily through dipolar interaction with the directly attached protons and to a lesser extent by chemical shift anisotropy (Abragam, 1961). Relaxation of a protonated ^{15}N spin is dependent on the spectral density function, $J(\omega)$ (Abragam, 1961; Lipari & Szabo, 1982a). Relaxation is dependent on molecular motion which is reflected in $J(\omega_i)$. The relaxation rates, R_1 and R_2, and steady-state NOEs of protonated ^{15}N nuclei are dependent on the values of $J(\omega_i)$ at five characteristic frequencies. In specific cases a contribution to the ^{15}N R_2 rate due to conformational or chemical exchange may contribute to the decay of transverse magnetization (McConnell, 1958; Woessner, 1961; Bloom et al., 1965). Thus, an R_{ex} term may be included in the final equation (Clore et al., 1990b; Stone et al., 1992).

The amplitudes and time scales of the internal molecular motions were determined using the model-free formalism (Lipari & Szabo, 1982a,b). Since, in general, there is insufficient experimental data to determine the five $J(\omega)$ values, the spectral density function for the molecular motion is approximated by

$$J(\omega_i) = (2/5)[(S^2\tau_m)/(1 + (\omega_i\tau_m)^2) + (1 - S^2)\tau/(1 + (\omega_i\tau)^2)] \quad (1)$$

S^2 is the generalized order parameter, which is a measure of the degree of spatial restriction of the unit bond vector (for the present study, the amide NH and tryptophan indole NH bonds) and $1/\tau = 1/\tau_m + 1/\tau_e$, where τ_m is the overall rotational correlation time of the molecule and τ_e is the effective internal correlation time describing rapid internal motions of the unit bond (τ_e reflects motions on the picosecond to nanosecond time scale). The value of S^2 ranges from 0, for unrestricted internal motion, to 1, for internal motion that is completely restricted, relative to the fixed molecular frame of reference of the macromolecule. In some cases it has been necessary to extend the model-free analysis to approximate motions on two time scales

(Clore et al., 1990a,b); then $S^2 = S^2_f S^2_s$, and S^2_f and S^2_s are the order parameters for the internal motions on fast and slow time scales, respectively. The effective correlation time for internal motions on the fast time scale is τ_f (τ_f < 500 ps), and τ_s is the effective correlation time for internal motions on an intermediate time scale ($\tau_f < \tau_s < \tau_m$).

Model-free parameters, obtained through back-calculation of the relaxation data for each resonance, were evaluated for five different dynamical models which contain a maximum of three variables. The five models and their associated dynamical variables are model 1 (S^2), model 2 (S^2 and τ_e), model 3 (S^2 and R_{ex}), model 4 (S^2, τ_e, and R_{ex}), and model 5 (S^2_f, S^2_s, and τ_e).

RESULTS

Spectra of the ^{15}N-DHFR−^{13}C-folate binary complex are essentially identical to those previously described (Falzone et al., 1994a). Figure 1A shows a ^{13}C-edited 600 MHz ^{1}H NMR spectrum of the ^{15}N-labeled DHFR−[^{13}C]-C_7,C_9-folate (1:6) complex. The relative concentration of apoenzyme present in solution is approximately 0.5% that of the binary complex. A single bound C_7-coupled ^{1}H resonance (pterin ring) is observed in the complex, at 9.77 ppm, which is absent from the apoenzyme spectrum and from the free folate spectrum (data not shown). The ^{1}H−^{15}N spectrum of the labeled binary complex (Figure 1B) suggests that the DHFR−folate complex adopts a single conformation, since only a single set of resonances is observed for each ^{15}NH group. At contour levels close to the base-plane noise, cross-peaks associated with apo-DHFR are not observed in the ^{1}H−^{15}N correlation spectrum of the binary complex (data not shown). Taken together, the spectra suggest that folate in the ^{15}N-labeled DHFR complex is bound in a single, productive conformation, as observed previously (Falzone et al., 1990, 1994a) and that any apoenzyme present is below detectable limits. If multiple protein conformations are present, as observed for the folate complexes of the *Lactobacillus casei* enzyme (Birdsall et al., 1987, 1989), then exchange between the various conformers must be fast on the chemical shift time scale to give a single, averaged set of resonances.

Of an expected 148 ^{1}H−^{15}N backbone cross-peaks for the DHFR−folate complex, 141 were assigned (Falzone et al., 1994a). In the present study, 108 cross-peaks were sufficiently well resolved in the ^{1}H−^{15}N correlated spectrum processed with 6 Hz line broadening in ω_2 for peak heights to be measured accurately (Figure 1B). An additional 10 cross-peaks were resolved in a resolution-enhanced spectrum processed using a Lorenztian−Gaussian transformation. Thus, reliable quantification of cross-peak intensity in the T_1, T_2, and {^{1}H}−^{15}N heteronuclear NOE experiments was possible for 118 of the protonated backbone ^{15}N atoms, including 93% (13 of 14) of the backbone NHs of residues in the folate binding site (I5, A6, A7, M20, W22, D27, L28, W30, F31, K32, I50, L54, and I94), the putative proton donor network (D27, Trp22 $N^{\epsilon 1}$), 89% (16 of 18) of the backbone NHs of residues in the NADPH binding site (I5, A6, A7, R44, T46, S63, K76, S77, V78, I94, G95, G96, V99, Y100, Q102, and T123), and 88% (14 of 16) of those in loop 1 (A9, V10, R12−M20, and W22−L24) (Bystroff et al., 1990).

Cross-peak heights in the heteronuclear correlation spectra were used to determine the ^{15}N relaxation time constants and {^{1}H}−^{15}N NOEs of the folate complex of DHFR. Peak height uncertainties were determined from duplicate spectra: uncertainties in the T_1 and T_2 data ranged from 1.1% to 5%; in the {^{1}H}−^{15}N NOE data the range was from 1.8% to 15%. As observed elsewhere (Stone et al., 1992), the variances in the peak heights were equal to the base-plane noise levels for the later time points of the T_2 experiment. For all time points in the T_1 experiment, and the earlier time points in the T_2 experiment, the peak height uncertainties were significantly greater than the rms noise levels.

Graphs of the peak heights of resonances plotted against the relaxation time and fitted by nonlinear regression to appropriate equations for T_1 and T_2 time constants indicate the relaxation data are of high quality (Figure 1C,D). For the T_1 data, χ^2 tests indicate curve fits for 113 of 118 resonances are adequate: For five resonances, peak height uncertainties are likely underestimated. A χ^2 test of the T_2 data indicates the curve fits for all backbone resonances are adequate.

^{15}N T_1, T_2, and NOE values and uncertainties are plotted versus residue number in Figure 2. Weighted mean values (Taylor, 1982) are as follows: T_1, 0.73 ± 0.0016 s (standard deviation = 0.006); T_2, 0.099 ± 0.0002 s (standard deviation = 0.0014); NOE, 0.79 ± 0.003 (standard deviation = 0.009). A wide range of backbone ^{15}N T_1 and T_2 values are observed (Figure 2A,B). For example (Figure 2B), T_2 values for 10 backbone NHs are greater than 8 standard deviations above the mean (M16, A19, W22, K38, G67, D69, V88, K106, E120, and G121). Similarly, a plot of {^{1}H}−^{15}N NOE versus residue number reveals that several regions of sequence exhibit NOEs that differ significantly from the mean (Figure 2C): G67, D69, and G121 are 9, 16, and 28 standard deviations, respectively, below the mean. Within each of the three ^{15}N relaxation experiments, the observed variations from the mean of many T_1, T_2, or NOE values are outside experimental error. Thus, we conclude that variations in the observed relaxation values are indicative of diverse dynamical features in the DHFR−folate complex.

Model-Free Analysis: Dynamical Model Selection Strategy. Method 1: An initial analysis [based on Clore et al. (1990a)] included τ_e in the dynamics calculation if the T_1/T_2 ratio for a given resonance was more than one sample deviation below the mean T_1/T_2 value, whereas R_{ex} was included if the T_1/T_2 ratio was more than one sample deviation above the mean (a τ_m value of 7.83 ns was estimated using a trimmed weighted mean T_1/T_2 ratio of 6.94 ± 0.030 (Kay et al., 1989; Clore et al., 1990a). Thus, we optimized S^2 and τ_e for 14 residues (model 2), S^2 and R_{ex} for 14 residues (model 3), and S^2 alone for 90 residues (model 1). However, the experimental data could not be back-calculated accurately, as judged by the high values of the optimization function, Γ_i (Figure 3A, legend). Thus, additional criteria were required to select dynamical parameters which would account for the relaxation data of the DHFR−folate complex.

We developed a six-step parameter selection protocol similar to that of Stone et al. (1992) which involved Monte Carlo simulations of possible τ_e or R_{ex} terms for each residue, optimization, and then comparison of the results from the Monte Carlo parameter selection to the results derived by method 1.

(a) Initially, 57 resonances were selected for which τ_e would be optimized. In this first calculation, S^2 and τ_e were

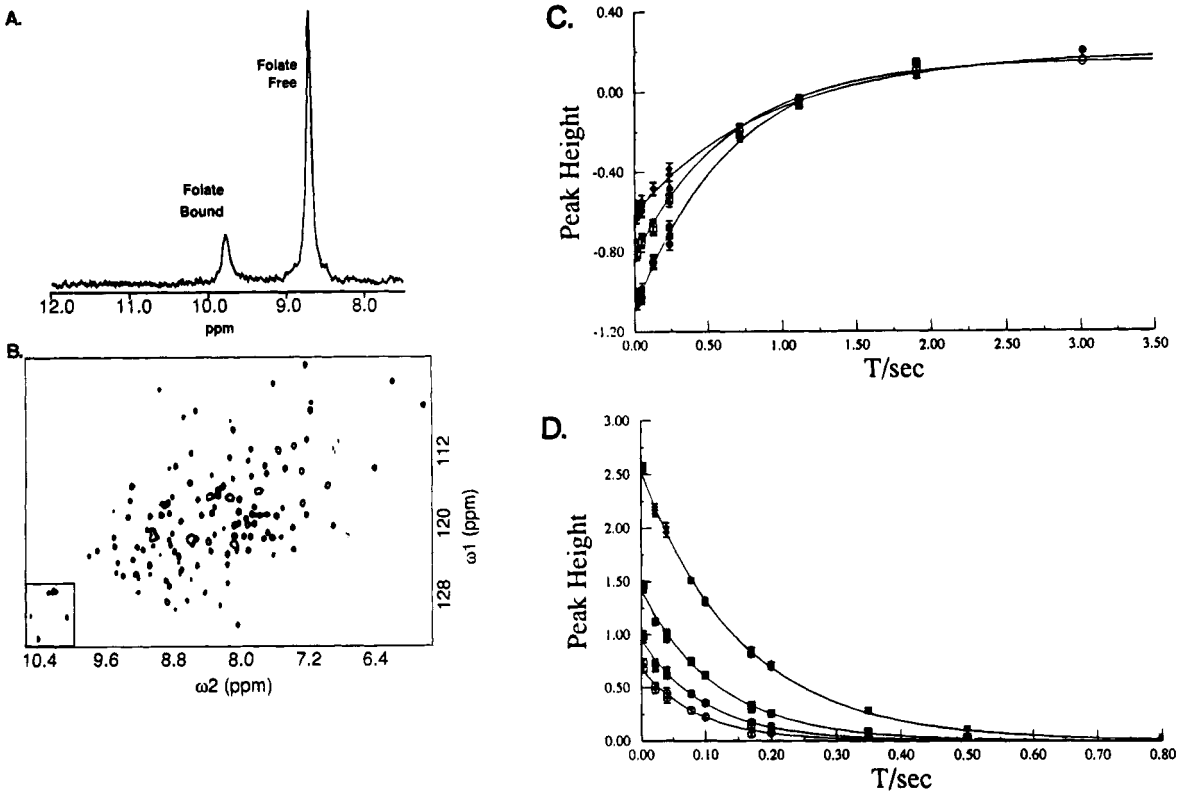

FIGURE 1: (A) ^{13}C-Edited 600 MHz ^1H spectrum of the 1:6 DHFR−folate complex. The spectral width in ω_2 was 12195.12 Hz, and 4096 real points were collected in ω_2 with the carrier placed on the residual $^2H^1H_2O$ resonance. A total of 2048 transients was collected. The ^{13}C carrier was set to the frequency of the folate C_7 resonance at 150 ppm. Carbon chemical shifts were referenced indirectly to TMS (Live et al., 1984; Bax & Subramanian, 1986). Spectra were processed with a 10 Hz line broadening in ω_2 (B) Typical $^1H-^{15}N$ contour plot, taken from the first T_2 experiment for the DHFR−folate complex. All relaxation experiments were performed by acquiring with 4096 × 128 complex points in $\omega_2 \times \omega_1$ dimensions, with a spectral width of 9259.26 Hz × 2127.66 Hz, respectively. In T_1 and T_2 experiments, 16 sensitivity-enhanced transients were collected; for NOE experiments 32 sensitivity-enhanced transients were acquired. For sensitivity-enhanced T_1 and T_2 experiments, the data sets obtained by deconvoluting the orthogonal magnetization components were combined. However, for the sensitivity-enhanced NOE experiments, data sets obtained by deconvoluting the orthogonal magnetization were treated independently. Quadrature detection in ω_1 was achieved using TPPI (Marion & Wuthrich, 1983). Short (0.5−1.5 ms) spin lock purge pulses were used for water suppression (Messerle et al., 1989). Decoupling of ^{15}N during acquisition was performed using the GARP-1 composite pulse decoupling sequence (Shaka et al., 1985) with a field strength of 1.25 kHz. The ^1H carrier was set to the frequency of the water resonance (4.73 ppm at 303 K); the ^{15}N carrier was set to 118.35 ppm. Nitrogen chemical shifts were referenced indirectly to liquid NH_3 (Live et al., 1984; Bax & Subramanian, 1986). Relaxation spectra were processed using two protocols. Protocol 1 was used to quantitate well-resolved cross-peaks; we used 6 Hz line broadening in ω_2; zero-filling once, a Lorenztian−Gaussian transformation followed by a 90° sine bell was applied in ω_1. Protocol 2 was used to quantitate moderately overlapped cross-peaks; a Lorenztian−Gaussian transformation was used in ω_2; ω_1 was transformed as in protocol 1. Simple spline baseline correction was employed in ω_2 in both protocols. The region in the lower right inset was processed by protocol 2. (C) T_1 relaxation curves for residues I2 (○), A9 (◆), and L54 (●). The longitudinal relaxation times were fit by a three-parameter nonlinear least squares fit of the equation $I(\mathbf{T}) = I_\infty - [I_\infty - I_0] \exp(-\mathbf{T}/T_1)$ to the experimental data. For T_1 measurement, 18 spectra were recorded using eight parametric relaxation delays of 0.017 (×3), 0.049 (×3), 0.128 (×3), 0.240 (×3), 0.716, 1.113 (×2), 1.906 (×2), and 3.018 s; parentheses indicate replicate experiments. (D) T_2 relaxation curves for residues W22 (■), L54 (●), V88 (◆), and D131 (○). The transverse relaxation times, T_2, were obtained by two- or three-parameter nonlinear fits, respectively, of the equations $I(\mathbf{T}) = I_0 \exp(-\mathbf{T}/T_2)$ or $I(\mathbf{T}) = I_\infty + I_0 \exp(-\mathbf{T}/T_2)$. I_∞ and I_0 are the initial and final cross-peak heights, respectively. For T_2 measurement, 18 spectra were recorded using 10 parametric relaxation delays of 0.004 (×2), 0.022 (×2), 0.040 (×2), 0.078 (×2), 0.100 (×2), 0.170 (×2), 0.200 (×2), 0.350 (×2), 0.500, and 0.800 s. Relaxation rate constants and NOE enhancements were calculated from cross-peak heights in the $^1H-^{15}N$ correlation spectra. The uncertainties in the measured peak heights, for all resolved cross-peaks, were estimated from replicate experiments. The standard deviation of the differences was divided by $\sqrt{2}$ to yield the uncertainty in the peak heights themselves (Palmer et al., 1991). Uncertainties in the relaxation rates are the standard errors in the fitted parameters. For those time points which were not duplicated, peak height uncertainties were estimated by interpolation of the uncertainties obtained for the repeated time points. Uncertainties in the relaxation data were verified by Monte Carlo simulations as described by Palmer et al. (1991). Curve fitting used the Levenburg−Marquardt algorithm (Press et al., 1986) to minimize the value of the χ^2 goodness-of-fit parameter, as described previously (Palmer et al., 1991; Stone et al., 1992, 1993). The sufficiencies of the monoexponential T_2 decay functions were evaluated with a χ^2 test, as previously described (Palmer et al., 1991). For the T_2 data, the significance of the improvement afforded by the three-parameter over the two-parameter equation was evaluated using an F statistic as described previously (Stone et al., 1992, 1993). Data for the T_2 measurements were fit with I_∞ included as a free parameter; for 115 resonances the experimentally determined value of I_∞ was equal to the random base-plane noise; thus I_∞ is equal to zero for most cases, and the two-parameter equation was adequate. Thus, two-parameter fitted T_2 values were selected for 115 resonances, and 3 resonances were fit using the three-parameter equation. Where the three-parameter fit is used, the I_∞ value was zero in two cases (F103 and D144) or equal to 3.9% of I_0, the initial cross-peak height (D131).

optimized for each resonance, R_{ex} values for all resonances were fixed at zero, and τ_m was fixed at 7.83 ns. For those resonances in which $\tau_e > 0$, τ_e was optimized in a final calculation. For all other resonances τ_e was fixed at zero.

(b) Second, 68 resonances were selected for which an R_{ex} term would be optimized. In this step, S^2 and R_{ex} were optimized for each resonance, all τ_e values were held at zero, and τ_m was set at the estimated value. For $R_{ex} > 0$, R_{ex} was

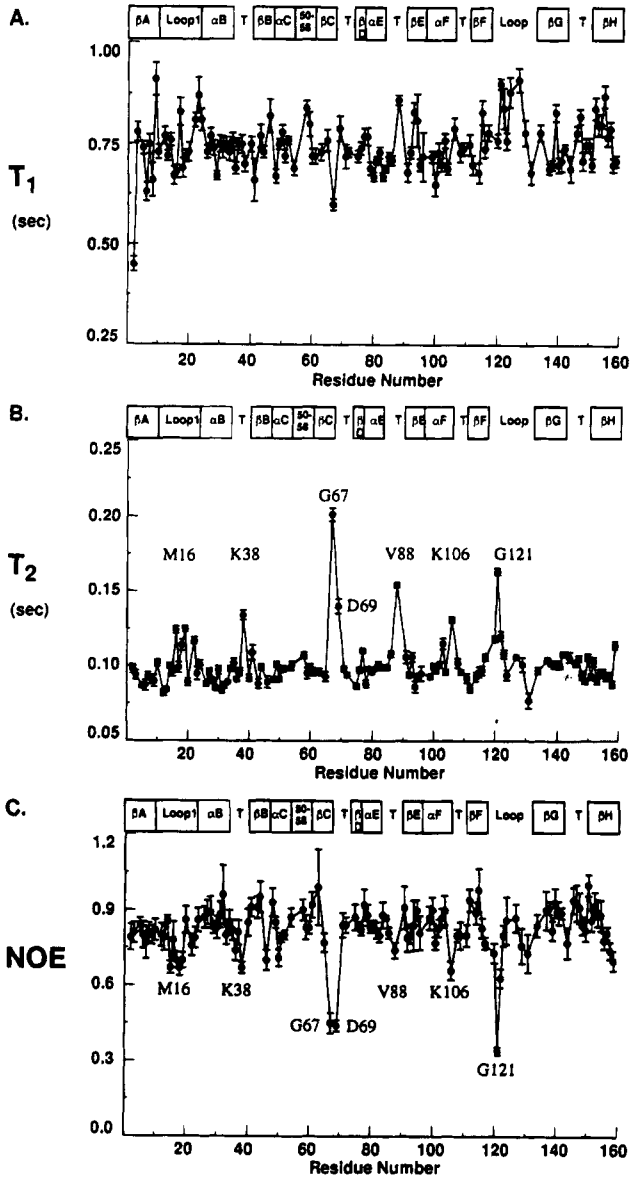

FIGURE 2: Relaxation data plotted for the 118 measured amide residues. Secondary structural elements of DHFR are shown above the individual plots. (A) T_1 values. Relaxation measurements were performed using inversion recovery for ^{15}N T_1 determination (Vold et al., 1968). T_1 values range from 0.45 to 0.9 s. (B) T_2 values. Measurements were performed using spin−echo CPMG sequences for ^{15}N T_2 determination (Meiboom & Gill, 1958). T_2 values range from 0.077 to 0.201 s. The T_1 and T_2 experiments consist of a refocused INEPT (Morris & Freeman, 1979; Barum & Ernst, 1980) sequence to transfer magnetization from the directly bound amide protons to the ^{15}N nuclei, a parametrically varied relaxation period, **T**, the t_1 evolution period, and a sensitivity-enhanced INEPT sequence to transfer magnetization from ^{15}N back to the proton for detection. To eliminate effects of dipolar cross-relaxation and cross-correlation between dipolar and CSA relaxation mechanisms on ^{15}N longitudinal relaxation (Boyd et al., 1990), proton decoupling (GARP-1; field strength 2 kHz) was applied during the relaxation period of the T_1 experiments. The CPMG sequence suppresses contributions from chemical exchange and scalar relaxation, if $k\delta \ll 1$, where k is the exchange or scalar relaxation rate constant and δ is the CPMG spin−echo time (Bloom et al., 1965). The interval 2δ between the refocusing pulses in the CPMG sequence was approximately 1 ms and is thus sufficiently short to spin-lock the ^{15}N spins. The effects of cross-correlation on ^{15}N transverse relaxation were eliminated by application of ^1H 180° pulses synchronously with every second echo in the CPMG sequence (Palmer et al., 1992; Kay et al., 1992). For T_1 and T_2 measurements, a recycle delay of 2 s was used between acquisitions. (C) $\{^1H\}-^{15}N$ NOE values. The NOE experiment was repeated in triplicate; thus, the three sensitivity-enhanced experiments afford six independent measurements which are used to determine NOE uncertainties (Stone et al., 1992). The steady-state $\{^1H\}-^{15}N$ heteronuclear NOEs were calculated as the ratio of peak heights in the spectrum recorded with proton saturation (plus NOE) to those in the spectrum recorded without saturation (no NOE). Thus, NOE values were determined by NOE = I_{sat}/I_{unsat}, in which I_{sat} and I_{unsat} are the peak intensities measured from the spectra acquired with and without amide proton irradiation during the recycle delay. Uncertainties in the NOE values, σNOE, were obtained from the uncertainties in the peak intensities (Stone et al., 1992). Measurements were performed using the steady-state NOE (Noggle & Shirmer, 1971). The experiment to measure the $\{^1H\}-^{15}N$ steady-state heteronuclear NOEs consist of an initial relaxation delay, with and without amide proton saturation, the t_1 evolution period, and a sensitivity-enhanced INEPT transfer of magnetization from the ^{15}N nuclei back to the proton for observation. The steady-state $\{^1H\}-^{15}N$ NOE was measured in an interleaved manner; hence, we alternately acquired no-NOE and plus-NOE transients. For measurements of the plus-NOE half of the steady-state $\{^1H\}-^{15}N$ NOE, 5 s of amide on-resonance low-power pulses was used (GARP-1; field strength 2 kHz), equivalent to 5.5 times the longest ^{15}N T_1 and approximately equal to the spin−lattice relaxation time constant for the water protons. For measurements of the no-NOE half of the steady-state $\{^1H\}-^{15}N$ NOE, the carrier was shifted 60 kHz downfield; CW field strength = 2 kHz.

optimized in a final calculation.

(c) Third, residues were excluded whose T_1/T_2 ratio was greater than 1.96 standard deviations from the mean. We optimized S^2 for each resonance, τ_m for the whole molecule, and τ_e and/or R_{ex} for the resonances selected from steps a and b.

(d) All 118 residues were included in the fourth calculation, and τ_m was optimized for the whole molecule. For resonances from step c for which the optimized τ_e and/or R_{ex} value equaled zero, the appropriate τ_e and/or R_{ex} term was fixed at zero (i.e., the simplest possible dynamical model was assumed). S^2 was optimized for each resonance, and τ_e and/or R_{ex} were optimized for the resonances selected from step c. The optimized τ_m value equaled 7.84 ± 0.02 ns, which converged from starting points of 6−12 ns. For 90 residues $\Gamma_i \simeq 0$. For 15 residues $5 < \Gamma_i < 20$: in these cases the back-calculated NOEs were about 10% lower than the experimental NOE, perhaps due to incomplete equilibration of H_2O proton magnetization during the heteronuclear steady-state NOE experiments (Grzesiek & Bax, 1993). Thus, for 105 residues the back-calculated data accurately predicted the experimental data. For 13 residues, Γ_i remained high; $45 < \Gamma_i < 450$ (step e, below).

(e) To fit the relaxation data for resonances with high residual (Γ_i) values, we compared the experimental data to back-calculated relaxation values. For these 13 residues (2, 16, 18, 19, 38, 67, 69, 88, 100, 106, 120, 121, and 159), differences between experimental and back-calculated data are greater than 10%, due, in general, to underpredicting the relaxation values. For example, back-calculated NOEs for residues 88, 16, 100, and 67 are 15%, 17%, 20%, and 40% lower than the respective experimentally determined NOEs. We then determined dynamical parameters for the remaining 13 residues using the extended spectral density function (Clore et al., 1990a,b; Stone et al., 1992; Akke et al., 1993) in which S^2_f, S^2_s, and τ_e are optimized with τ_m fixed at 7.84 ns: model 5 is sufficient to accurately describe the relaxation data for all 13 residues: for 12/13 residues, $\Gamma_i \simeq 0$; for I2, $\Gamma_i = 7.8$.

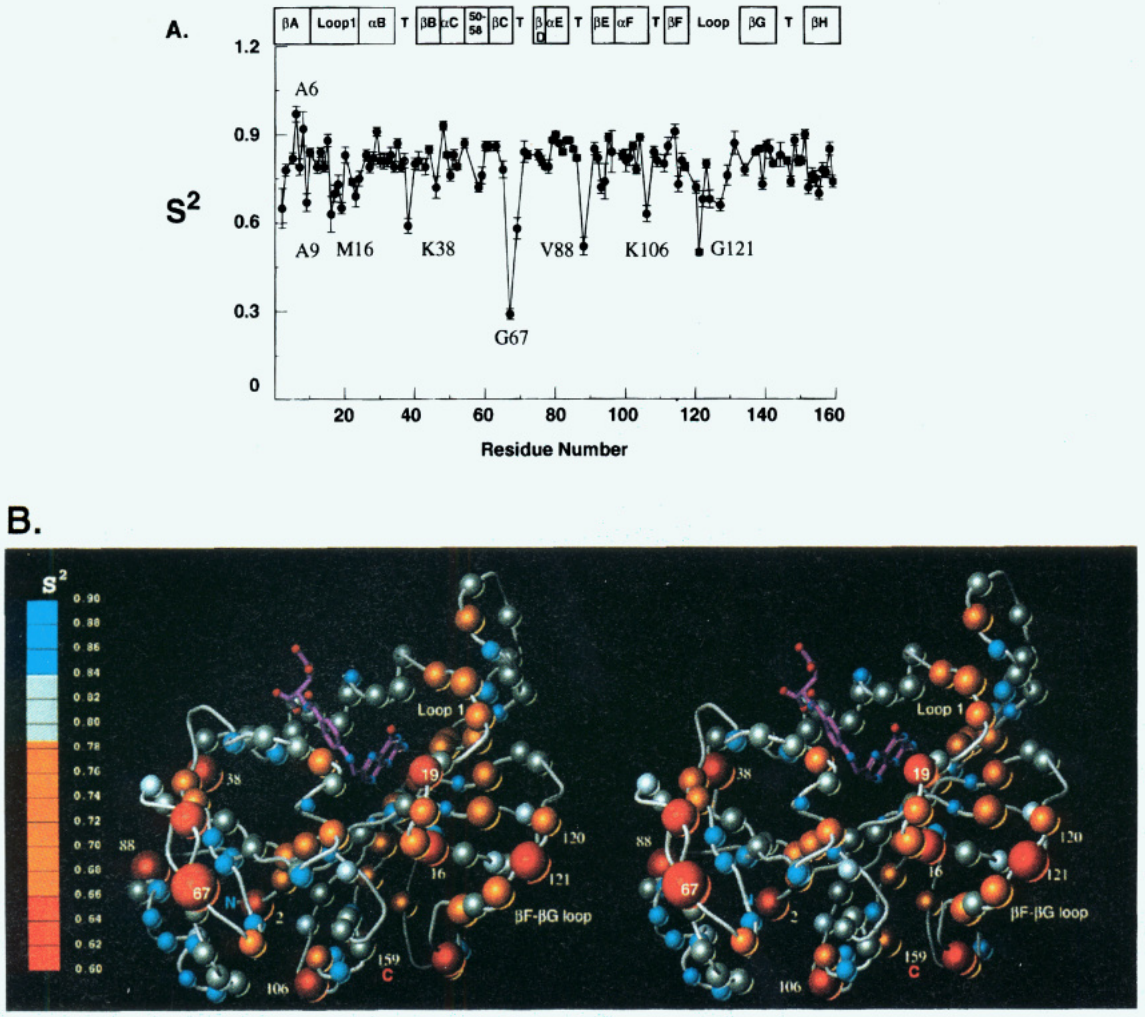

FIGURE 3: Backbone ^{15}N order parameters. (A) Generalized order parameters and uncertainties determined for the 118 backbone amide resonances in the DHFR−folate binary complex plotted versus residue number. The generalized order parameter is given by $S^2 = S^2_f S^2_s$, where S^2_f and S^2_s are the order parameters for the internal motions on fast and slow time scales, respectively. The secondary structural elements of DHFR are shown above the plot (Bolin et al., 1982). Calculation of the model-free parameters from the experimental data was performed by minimization of the target function $\chi_2 = \Gamma_i = [(R_{1i} - R_{1i}^*)^2/\sigma_{1i}^2 + (R_{2i} - R_{2i}^*)^2/\sigma_{2i}^2 + (\mathrm{NOE}_i - \mathrm{NOE}_i^*)^2/\sigma_{\mathrm{NOE}i}^2]$, in which Γ_i is the sum of the squared residuals; R_{1i}, R_{2i}, and NOE_i are the experimental values of the relaxation parameters ($R_1 = 1/T_1$ and $R_2 = 1/T_2$); σ_{1i}, σ_{2i}, and $\sigma_{\mathrm{NOE}i}$ are the uncertainties in the rate constants and NOEs; and R_{1i}^*, R_{2i}^*, and NOE_i^* are the values of the relaxation parameters back-calculated from the model-free dynamics parameters for the ith ^{15}N nucleus. The summation extends over all nuclei included in the calculation. Theoretical values were calculated utilizing the spectral density model chosen for each resonance (Results). (B) Amide ^{15}N S^2 values are shown mapped onto the X-ray crystal structure (Bolin et al., 1982) of the DHFR−MTX complex. Folate has been modeled into the active site in place of MTX using AVS. The volume of each sphere is inversely proportional to its individual S^2 value. Sphere color is scaled as follows: the weighted mean S^2 value and standard deviation for the DHFR−folate complex is 0.81 ± 0.0085; silver spheres represent S^2 values within 3 standard deviations of the mean (99.7% confidence limit), i.e., $0.78 \leq S^2 \leq 0.83$; blue spheres, $0.84 \leq S^2 \leq 1.0$; orange spheres, $0.67 \leq S^2 \leq 0.77$; red spheres, $0.25 \leq S^2 \leq 0.65$. Residues for which no data are available are not shown.

(f) We then compared the fits obtained using the Monte Carlo method to those of method 1. Fifty-two resonances were fit adequately using the dynamical models selected in method 1, and thirteen were fit better by models selected from method 1 than the Monte Carlo method. Thus, in these cases the simpler model was chosen. However, for the majority of residues, fits to the experimental data improved significantly (within 95% confidence limits) using the Monte Carlo method.

According to these selection criteria, the ^{15}N T_1, T_2, and NOE relaxation data for the 118 backbone NHs of the DHFR−folate binary complex are accurately described using model 1 (S^2) for 34 residues, model 2 (S^2 and τ_e) for 6 residues, model 3 (S^2 and R_{ex}) for 45 residues, model 4 (S^2, τ_e, and R_{ex}) for 20 residues, and model 5 (S^2_f, S^2_s, and τ_e) for 13 residues (supporting information).

A plot of generalized S^2 values versus residue number reveals that, indeed, diverse dynamical features are evident in the folate complex (Figure 3A). The weighted mean S^2 value is 0.81 ± 0.0015. Several resonances have S^2 values which are significantly outside the mean. The weighted mean backbone S^2 value of residues which comprise the occupied folate binding site is 0.80 ± 0.006 (includes backbone NHs of I5, A6, A7, M20, W22, D27, L28, W30, F31, K32, I50, L54, and I94). Whereas, for the residues which comprise the unliganded NADPH site, the weighted mean S^2 is 0.83 ± 0.004 (includes backbone NHs of I5, A6, A7, R44, T46, S63, K76, S77, V78, I94, G95, G96, V99, Y100, Q102, and T123). This suggests the backbone comprising the unoccupied cofactor binding site is at least as conformationally restricted as that of the occupied folate site, on the picosecond time scale.

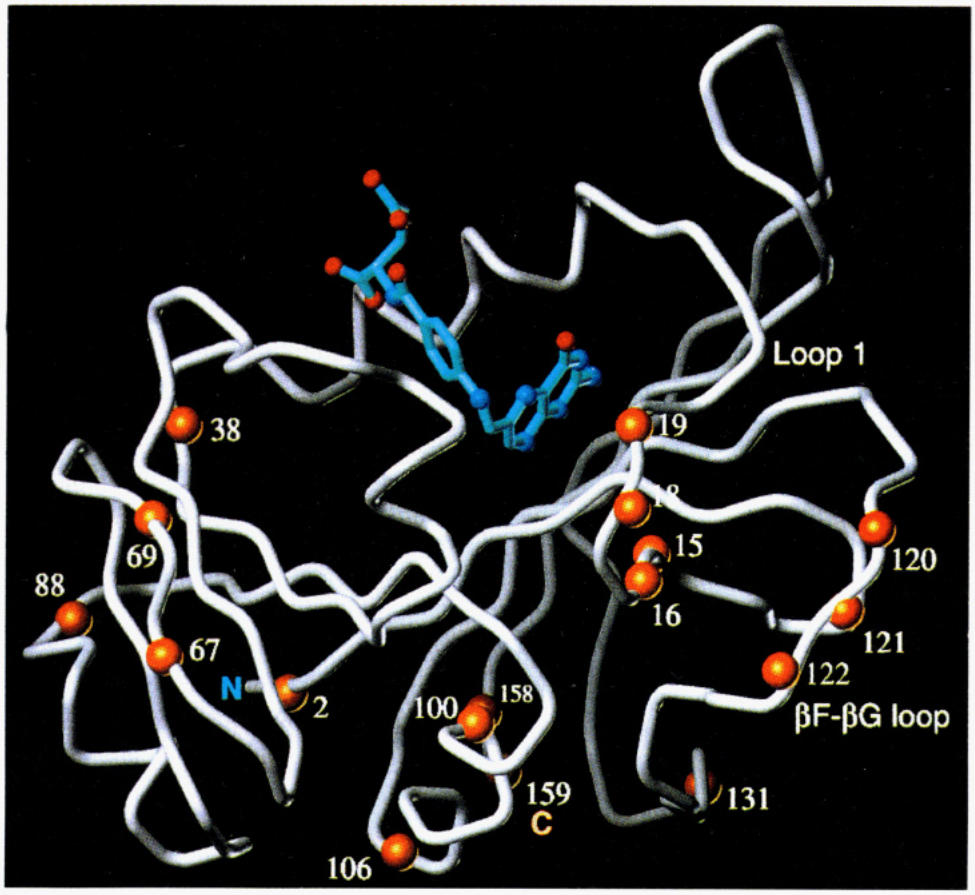

FIGURE 4: Map of the effective correlation time (τ_e) for internal motions, on the picosecond to nanosecond time scale, for the backbone amide nitrogens of the DHFR−folate complex. Residue-specific τ_e and generalized S^2 values (in parentheses) are I2, 6051 ± 2081 ps (0.65); G15, 81 ± 24 ps (0.88); M16, 3894 ± 5438 ps (0.63); N18, 1128 ± 296 ps (0.73); A19, 1595 ± 325 ps (0.65); K38, 1720 ± 210 ps (0.59); G67, 1610 ± 120 ps (0.29); D69, 729 ± 136 ps (0.58); V88, 2350 ± 692 ps (0.52); Y100, 4904 ± 3188 ps (0.81); K106, 1061 ± 266 ps (0.63); E120, 1100 ± 425 ps (0.72); G121, 614 ± 48 ps (0.50); D122, 30 ± 6 ps (0.68); D131, 40 ± 30 ps (0.87); R158, 32 ± 13 ps (0.85); R159, 1111 ± 320 ps (0.74).

It is important to consider the reliability of the τ_e values determined for the 39 residues from models 2, 4, and 5. Calculated τ_e values may be unreliable since precision is dependent on S^2: in general, low uncertainty in τ_e is observed for resonances exhibiting low S^2 values (Lipari & Szabo, 1982a; Palmer et al., 1991). We assessed the reliability of the τ_e values by performing model-free calculations in which Γ_i is determined from a series of fixed τ_e values (Stone et al., 1993). For most resonances in the DHFR−folate complex τ_e values were less than 30 ps and were found to be unreliable. However, for 17 residues (Figure 4) graphs of Γ_i versus τ_e revealed well-defined minima (data not shown), thus indicating motions occurring on the 30 ps to 6 ns time scale. For 13 of 17 residues, τ_e values were determined using the two-time scale spectral density equation (model 5) and ranged from 0.6 to 6 ns (Figure 4). Our data suggest that, in general, τ_e values were well determined for residues whose S^2 values ranged from 0.29 to 0.74, although residues G15, Y100, D131, and R158 exhibit S^2 values greater than 0.80 as well as high τ_e values (Figure 4). Due to the uncertainties discussed above, it is not justified to quantitatively interpret the absolute value of τ_e for a given NH bond. Rather, the τ_e data taken together with the S^2 values suggest that motions are indeed occurring in the protein backbone within the picosecond to nanosecond time scales. The data therefore indicate that high frequency motions on the picosecond and nanosecond time scale occur in the DHFR−folate complex at sites within the βA−αB (loop 1) and the βF−βG loops, between the adenosine binding domain and the major domain, within the adenosine binding domain, and at the N- and C-termini (Figure 4).

Graphs showing the dependency of Γ_i on variation in R_{ex} (Stone et al., 1993) revealed well-defined minima (data not shown). R_{ex} values were determined for 65 resonances (Figure 5A), 58 of which have R_{ex} values greater than 1 s^{-1}. The mean R_{ex} value is 1.5 ± 0.05 s^{-1}, and three residues have R_{ex} values greater than 3 s^{-1}. Thus, the relatively large R_{ex} values for the complex suggest there are microsecond to millisecond time scale motions leading to ^{15}N conformational exchange. Exchange-broadened residues are clustered in several β-strands, the αB helix, and around the folate binding site (Figure 5B).

Tryptophan Side Chain Indole NH. Relaxation data and model-free parameters (calculated using a chemical shift anisotropy of −89 ppm (Cross & Opella, 1983) for the five side-chain indole NH groups of the DHFR−folate complex are tabulated in supporting information. Generalized S^2 values for the indole $N^{\epsilon 1}$ are 0.91 ± 0.02 (W22), 0.97 ± 0.04 (W30), 0.85 ± 0.01 (W47), 0.95 ± 0.02 (W74), and 0.90 ± 0.04 (W133). The W30 indole ^{15}N resonance exhibited exchange line broadening, for which an R_{ex} of around 2 s^{-1} was determined. Although backbone ^{15}N relaxation data could only be quantitated for W22 and W30, the data suggest that, in general, the fast time scale motions

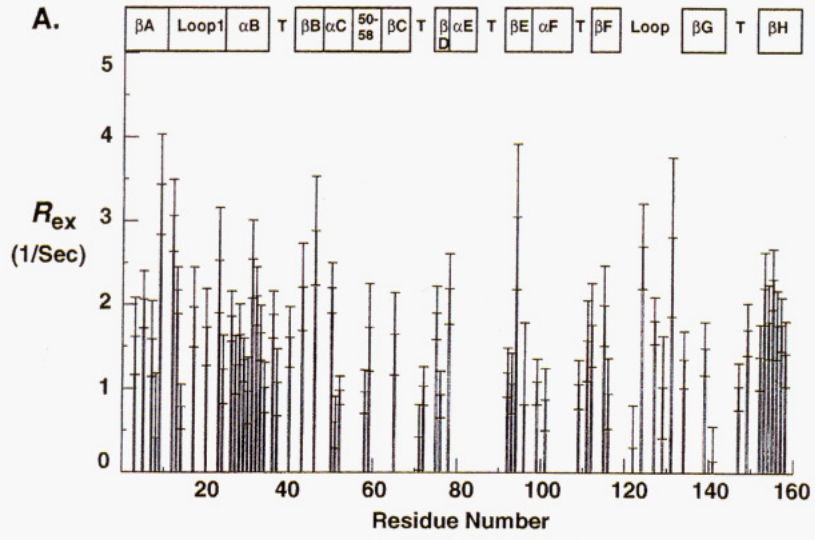

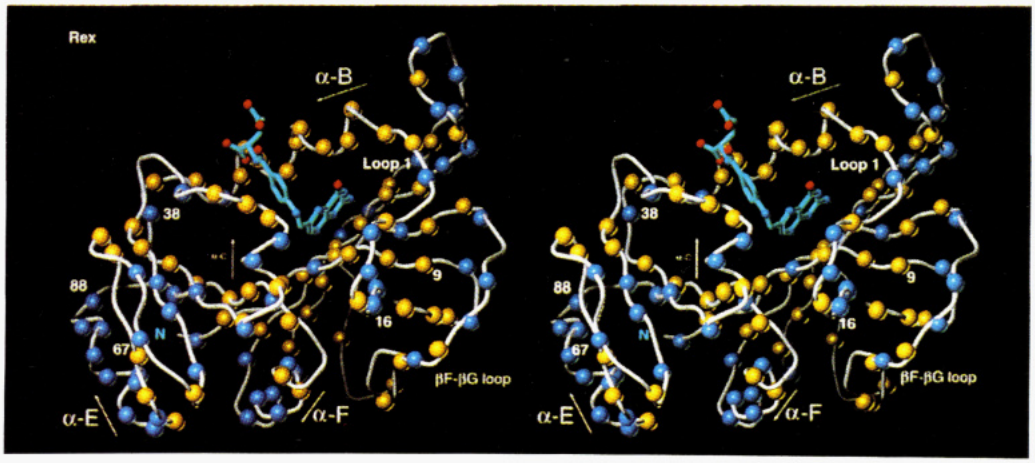

FIGURE 5: ^{15}N exchange contribution to T_2 relaxation for backbone amide nitrogens. (A) R_{ex} values determined for the backbone amide resonances in the DHFR−folate binary complex are plotted versus residue number. (B) Residues for which an R_{ex} value was determined are shown mapped onto the crystal structure-based model of the DHFR−folate complex. The 65 NH resonances exhibiting R_{ex} values are shown as yellow spheres. Blue spheres indicate an R_{ex} value of zero. Resonances for which no data are available are not shown.

of the tryptophan side chains are of lower amplitude than those of the corresponding backbone NH, presumably reflecting tight packing in the interior of the protein.

DISCUSSION

The backbone and tryptophan indole side-chain dynamics of the DHFR−folate binary complex were investigated by ^{15}N nuclear spin relaxation. Previous NMR studies (Falzone et al., 1990, 1991, 1994a) of this system demonstrate that the orientation of the pterin ring in bound folate is identical to that in an active complex predicted from structures of the DHFR−folate−$NADP^+$ ternary and DHFR−folate binary complexes (Bystroff et al., 1990; Reyes et al., 1995). Thus, the backbone dynamics of a productive enzyme−substrate analog complex were investigated. Meaningful results from such a ^{15}N spin relaxation study are obtained if one can determine, with high confidence, appropriate dynamical models for calculating the amplitudes and time scales of internal motion. We have shown through rigorous analysis of the back-calculated data that the dynamical parameters determined in this study accurately predict the experimental relaxation data. The experimental data (Figure 2) demonstrate that the ^{15}N relaxation times and $^1H-^{15}N$ NOEs for several regions of DHFR are significantly different than those of the mean for the molecule. The dynamical parameters derived using the Lipari−Szabo model-free approach (Lipari & Szabo, 1982a,b) indicate that diverse time-dependent fluctuations are indeed evident in the DHFR−folate complex. Structural fluctuations occur in important catalytic sites and at sites involved in ligand-dependent conformational change (Figures 3−5).

DHFR is composed of an eight-stranded β-sheet, four α-helices, and five loops and is divided into two structural domains separated by a hinge (Bystroff & Kraut, 1991; Brown & Kraut, 1992). The major domain (residues 1−37 and 89−159) contains the folate binding site and three surface loops. The smaller domain is denoted as the adenosine binding domain (residues 38−88). The active site is a 15 Å deep cavity lined with hydrophobic side chains and containing the carboxyl side chain of D27 (Bolin et al., 1982). The catalytic role of D27 in the requisite proton transfer to N_5 of H_2F has been evaluated through mutagenic, kinetic, and structural analyses (Howell et al., 1986; Fierke et al., 1987; Brown & Kraut, 1992; Basran et al., 1995). Backbone atoms of three residues (I5, A6, and A7) make van der Waals contact with both the substrate and cofactor

(Bolin et al., 1982; Bystroff et al., 1990; Brown & Kraut, 1992).

Relevance to DHFR Catalysis. Salient mechanistic features of DHFR are rate-limiting tetrahydrofolate (H_4F) release under steady-state conditions, pH 6−7, and rebinding of NADPH in place of $NADP^+$ prior to H_4F release (Fierke et al., 1987). Thus, in DHFR, as with many other enzymes, physical rather than chemical processes limit reaction rates (Cleland, 1975). Biochemical events in DHFR such as enzyme turnover, substrate and cofactor binding or dissociation, and conformational change occur at rates which range from 10 to 1000 s^{-1} (Fierke et al., 1987): close to the time scale of motions which may affect R_{ex}. Hence, rapid interconversion between conformational substates within regions of the active site may affect function. The important question is whether fluctuations at any particular site in DHFR affect substrate specificity or rate enhancement?

Folate and Cofactor Binding Sites. Of mechanistic interest are the dynamical parameters of the backbone NHs of residues which comprise the substrate and cofactor binding sites. The mean S^2 values are approximately equal ($S^2 \sim 0.80$) for residues comprising the occupied folate site and for the entire amide backbone of the DHFR−folate complex. This suggests that the high frequency (10^9−10^{12} s^{-1}) motions of the folate site are close to the average for the entire NH backbone and correspond to backbone torsion angle fluctuations of ~18° (Brüschweiler & Wright, 1994). Residues exhibiting the highest S^2 values within the active site are A6, L54, and G95 ($S^2 = 0.97$, 0.87, and 0.89, respectively). The lowest S^2 value in the folate site is 0.74 for the backbone NH of W22, corresponding to torsion angle fluctuations of only ~20°. The high S^2 values for the active site tryptophan indole side-chain NHs for W22 and W30 (0.91 and 0.97, respectively) further indicate considerable motional restriction for both the backbone and bulky tryptophan side chains in the folate site. We infer that the folate binding site is rigid on the picosecond to nanosecond time scales, at least in the presence of folate.

It is of interest to compare the average motional fluctuations of the occupied folate site to those of the empty cofactor binding site. Folates and cofactors bind cooperatively to DHFR, with folate binding inducing structural changes in both the adenosine binding domain and the NADPH binding site (Bolin et al., 1982; Bystrof & Kraut, 1991). Cofactor and substrate binding sites overlap such that the nicotinamide and pterin moieties bind in the same region (Brown & Kraut, 1992). We find that the mean backbone S^2 values of the occupied folate site and the empty NADPH site are essentially equivalent, $S^2 \sim 0.80$. Of note is K106, a turn residue at the end of helix αF (NADPH binding site), which is mobile ($S^2_f = 0.74$) on the picosecond to nanosecond time scale; possible relevance of its flexibility to catalysis is not known. Thus, even in the absence of cofactor, the empty binding site is relatively immobile on the picosecond to nanosecond time scale.

It is not known whether backbone or side-chain dynamical parameters are related to cooperative binding effects in DHFR nor whether folate binding serves to reduce mobility of the active site region, in addition to its role in altering loop 1 dynamics (Falzone et al., 1990, 1994b). However, the results of the present analysis provide an important foundation for further investigation. It is of interest that ligand binding may induce order into both the empty cofactor and the folate sites, since under certain conditions the reduction of mobility in an enzyme active site is a mechanism for increasing substrate specificity and reaction rate through an induced-fit conformational change (Herschlag, 1988). In contrast, it has been postulated that conformational flexibility, as evidenced through slow exchange processes and ligand dynamics for the *L. casei* dihydrofolate reductase, plays a role in determining substrate specificity [reviewed in Roberts (1991)].

It is of interest in light of the evidence for relatively low amplitude, high frequency motions in the folate site that slow conformational fluctuations on the microsecond to millisecond time scale are evident in the R_{ex} terms for many residues clustered around the folate site and within the β-sheet (Figure 5). Of particular interest is the entire αB helix, for which the backbone appears to exhibit slow time scale motions. Further, the side chain of W30 in the center of αB is also significantly ^{15}N exchange broadened, indicating that motions of both the backbone and indole side chain are occurring in the microsecond to millisecond regime. The clustering of exchange-broadened backbone NHs extends, in register, across the sheet (Figure 5B). These slower time scale motions likely occur within the DHFR−folate binary complex itself.

R_{ex} terms arise from conformational exchange processes within the folate complex itself through protein or ligand conformational rearrangements. Folate exchange or exchange between apo-DHFR and the DHFR−folate complex does not contribute significantly to R_{ex}. To affect T_2, exchange processes must occur on the time scale of the delay between refocusing pulses in the CPMG sequence. Contributions from exchange processes are suppressed if $k\delta < 1$, where k is the exchange rate and δ is the CPMG spin−echo time (1 ms in the present work) (Allerhand & Gutowsky, 1964; Bloom et al., 1965). The ^{15}N exchange rate must therefore be around 1000 s^{-1} to contribute to R_{ex}. Since the folate exchange rate is around 30 s^{-1} (Epstein and Boulat, unpublished data), this rate should not contribute to R_{ex}. The magnitude of the line broadening reflected in R_{ex} depends upon the resonance frequency difference between ^{15}N conformers, equilibrium populations of the conformers, and the exchange rates between species (Luz & Meiboom, 1963; Allerhand & Gutowsky, 1964, 1965; Gutowsky et al., 1965). The effect of an exchange process arising from free and bound folate may be examined by considering the contribution to line width from exchange between apo and binary DHFR enzyme states, given by (Luz & Meiboom, 1963; Allerhand & Gutowsky, 1964)

$$R_{ex} = k_{ex}^{-1}[1 - (2/(\delta k_{ex}))(\tanh(\delta k_{ex}/2))][P_{apo}P_{binary}(\omega_{ex}^2)] \quad (2)$$

where k is the exchange rate; δ is the CPMG spin−echo time; P_{apo} and P_{binary} are the mole fraction of apo and binary conformers, respectively; $\omega_{ex}^2 = [\omega(\text{apo-DHFR}) - \omega(\text{DHFR−folate})]^2$ and ω(apo-DHFR) and ω(DHFR−folate) are the Larmor frequencies of the spin in the apo and binary states, respectively. A measurable R_{ex} value requires that k_{ex} be on an appropriate time scale *and* that the sampled conformers have large enough ^{15}N chemical shift differences to yield detectable line broadening (eq 2); therefore, residues for which R_{ex} is zero may still be mobile on the microsecond to millisecond time scale. Simulations of R_{ex} as a function

of folate exchange rate and ^{15}N ω_{ex} values (60−600 Hz) indicate that the slow folate exchange cannot contribute to line broadening under the conditions of our experiments (data not shown). ^{15}N line broadening does not arise, therefore, from exchange between a small equilibrium population of apo-DHFR and the DHFR−folate binary complex. Taken together, this analysis suggests the R_{ex} terms arise from exchange between distinct enzyme conformers of the DHFR−folate binary complex. Motions of protein side chains, movement of secondary structural elements, or rotations of the pterin ring or *p*-aminobenzoyl portion of bound folate are mechanisms which may contribute to R_{ex}. We note that apo-DHFR interconverts between two equilibrium conformers, termed E_1 and E_2, at a rate of 0.035 s^{-1} (Cayley et al., 1981; Fierke et al., 1987). On the chemical shift time scale, only one conformer, likely E_1, is resolved in the DHFR−folate binary complex (Falzone et al., 1994a). Exchange between the E_1 and E_2 states is too slow to contribute to R_{ex}.

Thus, our study indicates that the occupied folate site exhibits limited high frequency motions but undergoes significant conformational fluctuations occurring at rates between 10^3 and 10^6 s^{-1}. However, not all residues which surround the occupied folate site show R_{ex} terms. As noted above, this does not rule out motions on the microsecond to millisecond time scale, since the ^{15}N chemical shift differences between the sampled conformations may be too small to lead to discernible line broadening.

The ^{15}N relaxation data for the binary complex indicate restricted backbone mobility, on the slower time scale, for residues 16−19 in loop 1 (Figure 5). In contrast, loop 1 displays millisecond time scale mobility in the apoenzyme (Falzone et al., 1994b). The ^{15}N dynamics data are thus consistent with the structural evidence that, upon folate binding, loop 1 encapsulates the active site. Whereas in both apo and $NADP^+$ binary states the central region of the loop is disordered (Bystroff & Kraut, 1991) in the ternary complex, two turns within loop 1 (residues 9−12 and 16−19) are ordered and contact the pterin ring of the substrate and the nicotinamide moiety of NADPH (Bystroff et al., 1990).

It is of interest, then, that residues 16−19, necessary for optimal hydride transfer (Li et al., 1992), exhibit nanosecond time scale structural fluctuations (Figures 3 and 4). Low order parameters ($S^2 = 0.6$) and high τ_e vlaues (1−4 ns) are observed in the central part of loop 1 (residues 16−19), even though loop 1 encapsulates the active site. Thus, for the DHFR−folate complex, the induced-fit conformational change does not completely abrogate high frequency motions in the central portion of loop 1. The high frequency motions in loop 1 of the binary complex may be reduced even further as new interactions are formed in the ternary complex and in the hydride transfer transition state.

βF−βG Loop. A subtle ligand-dependent conformational change has been observed in the βF−βG loop (Figure 6) which, upon folate binding, collapses inward toward loop 1 (Bystroff & Kraut, 1991). Figures 3 and 4 indicate that large amplitude ($S^2 = 0.5−0.7$) motions on the nanosecond time scale ($\tau_e = 0.6−1$ ns) are present in the central portion of the βF−βG loop (residues 120−124). As in loop 1, lower frequency motions are essentially absent from the βF−βG loop (Figure 5). The ligand-dependent conformational change evident in the central portion of the βF−βG loop

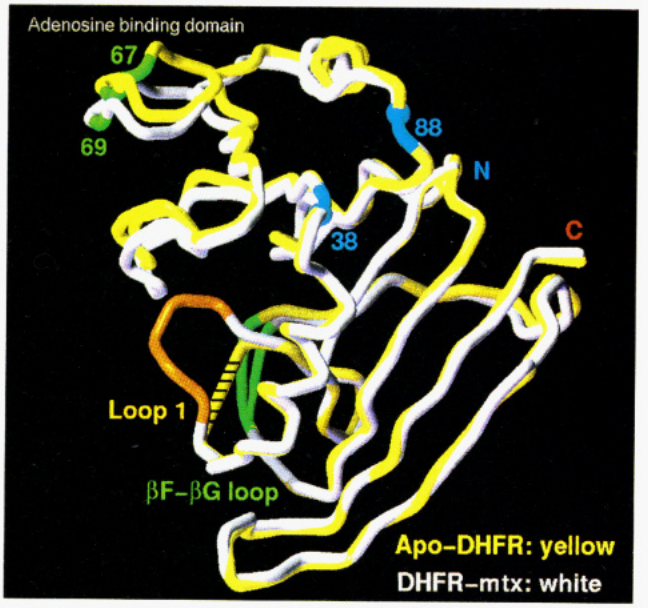

FIGURE 6: Conformational changes in DHFR indicated by X-ray crystal structures. The backbone of the DHFR−MTX complex (white) is shown superimposed over that of the apo-DHFR structure (yellow) (Bystroff et al., 1990; Bystroff & Kraut, 1991). The orientation of DHFR in this figure is adapted from Bystroff and Kraut (1991). The two structures are superimposed to give a best fit for the major domain, residues 1−37 and 89−159; the adenosine binding domain, residues 38−88, is then out of register due to ligand-driven movement of the two domains relative to one another. Loop 1, residues 16−24, is disordered in the apo and $NADP^+$ binary complex structures, as indicated by hatch marks but becomes ordered in the MTX binary and folate−$NADP^+$ ternary complexes (orange). Residues designated as the hinge (Bystroff & Kraut, 1991) between the adenosine binding domain and the major domain are K38 and V88 (blue). Conformational differences between the two structures are also noted in the βF−βG loop (green), residues 120−122. Residues G67 and D69, of the adenosine binding domain, are also indicated in green.

and its proximity to loop 1 and to the active site suggest the high frequency motions here might be mechanistically significant. Flexible loops proximal to protein active sites have been observed through ^{15}N relaxation analysis in enzyme IIa (Stone et al., 1992), thioredoxin (Stone et al., 1993), FKBP (Cheng et al., 1994), and *E. coli* RNase H (Mandel et al., 1995).

Adenosine Binding Domain. Bystroff and Kraut (1991) propose that, upon MTX binding, residues between the cofactor and substrate binding crevices act as a hinge about which the major domain and the adenosine binding domain rotate (Figure 6). Similar movement is observed in other folate−analog complexes of DHFR (K. Brown, personal communication; Reyes et al., 1995) and, thus, is not due to crystal packing effects. Data for the binary complex do not indicate differences in fast time scale mobility between the major domain and the adenosine binding domain. As to the slower time scale, we note that fewer exchange-broadened residues are located in the adenosine binding domain (14 of 35, 40%) than in the major domain (51 of 83, 60%). The ^{15}N relaxation data shed light upon backbone dynamics occurring between the adenosine binding domain and the major domain. Residues K38 and V88, which comprise the putative hinge between the adenosine binding domain and the major domain, exhibit high amplitude, nanosecond time scale motions. The S^2 values for K38 and V88 (~0.55) correspond to dihedral angle fluctuations of ~35°, and the

τ_e values are 1.7 and 2.3 ns, respectively (Figures 3 and 4). If the backbone at residues K38 and V88 indeed functions as a hinge, then hinge flexibility is maintained in the form of high frequency motions, even in the presence of folate.

Other Flexible Sites. Other regions in DHFR also exhibit low order parameters and fast time scale motions (Figures 3 and 4) and are noted here for completion. Residue G67 exhibits the lowest order parameter of the molecule (S^2 = 0.29, corresponding to dihedral angle fluctuations of ~50° (Brüschweiler & Wright, 1994). Residues G67, which lies within a surface loop, and D69 (S^2 = 0.58), which lies within a turn, in the adenosine binding domain (Figures 3 and 4) have not been implicated in catalysis by either biochemical or structural means, and the functional significance of this flexibility is at present unknown.

CONCLUSIONS

Analysis of the S^2 and τ_e data indicates that dynamic fluctuations occurring on the picosecond to nanosecond time scale, of potential relevance to catalysis, are limited to residues clustered in loop 1 and in the βF−βG loop and to sites comprising the "hinge" between the adenosine binding domain and the major domain. The clustering of residues with low order parameters in the loop regions of DHFR is consistent with correlated motion occurring on a fast time scale within loop 1 and also within the βF−βG loop. It is of significant interest that fast time scale backbone motions occur in regions of loop 1 which are implicated, from mutagenesis and kinetic data (Li et al., 1992), in transition-state stabilization. Furthermore, it is of interest that high frequency motions occur in DHFR in regions implicated, from X-ray data (Bystroff & Kraut, 1991), in ligand-dependent conformational changes between the apoenzyme, binary, and ternary complexes.

Analysis of the R_{ex} data indicates that many residues exhibiting dynamic fluctuations on the slower time scale are located around the DHFR folate binding site. We suggest that these apparent slow time scale motions are due to conformational fluctuations within the DHFR−folate binary complex. The apparent clustering of residues in the β-strands and αB helix which are ^{15}N exchange broadened is consistent with correlated motions on the slower time scale.

We conclude that the observed time-dependent structural fluctuations of the binary complex are indeed associated with the catalytic properties of the molecule, including ligand-dependent conformational changes and ligand binding.

ACKNOWLEDGMENT

We thank Dr. Arthur G. Palmer, III, for providing software and Drs. Martin J. Stone, Ishwar Radhakrishnan, Mark Rance, John Cavanagh, and Katherine A. Brown for helpful discussions. For molecular graphics, we gratefully acknowledge the expertise of Mike Pique.

SUPPORTING INFORMATION AVAILABLE

Table 1 giving ^{15}N relaxation data for the DHFR−folate complex, Table 2 giving backbone dynamical parameters for the DHFR−folate complex, and Table 3 giving dynamical parameters of the tryptophan indole $N^{\epsilon 1}$ for the DHFR−folate complex (15 pages). Ordering information is given on any current masthead page.

REFERENCES

Abragam, A. (1961) *Principles of Nuclear Magnetism*, pp 264−353, Clarendon Press, Oxford.
Akke, M., Skelton, N. J., Kordel, J., Palmer, A. G., & Chazin, W. J. (1993) *Biochemistry 32*, 9832.
Allerhand, A., & Gutowsky, H. S. (1964) *J. Chem. Phys. 41*, 2115.
Allerhand, A., & Gutowsky, H. S. (1965) *J. Chem. Phys. 42*, 1587.
Baccanari, D. P., Phillips, A., Smith, S., Sinski, D., & Burchall, J. (1975) *Biochemistry 14*, 5267.
Baccanari, D. P., Averett, D., Briggs, C., & Burchall, J. (1977) *Biochemistry 16*, 3566.
Barbato, G., Ikura, M., Kay, L. E., Pastor, R. W., & Bax, A. (1992) *Biochemistry 31*, 5269.
Basran, J., Casarotto, M. G., Barsukov, I. L., & Roberts, G. C. K. (1995) *Biochemistry 34*, 2872.
Bax, A., & Subramanian, S. J. (1986) *J. Magn. Reson. 67*, 565.
Bennett, W. S., & Steitz, T. A. (1980) *J. Mol. Biol. 140*, 211.
Birdsall, B., Feeney, J., Tendler, S. J., Hammond, S., Searle, M. S., Roberts, G. C. K., Colwell, W. T., & Crase, J. (1987) *FEBS Lett. 217*, 106.
Birdsall, B., DeGraw, J., Feeney, J., Hammond, S., & Roberts, G. C. K. (1989) *Biochemistry 28*, 2297.
Bloom, M., Reeves, L. W., & Wells, E. J. (1965) *J. Chem. Phys. 42*, 1615.
Bolin, J. T., Filman, D. J., Matthews, D. A., Hamlin, R. C., & Kraut, J. (1982) *J. Biol. Chem. 257*, 13650.
Boyd, J., Hommel, U., & Campbell, I. D. (1990) *Chem. Phys. Lett. 175*, 477.
Brown, K. A., & Kraut, J. (1992) *Faraday Discuss. 93*, 217.
Brüschweiler, R., & Wright, P. E. (1994) *J. Am. Chem. Soc. 116*, 8426.
Burum, D. P., & Ernst, R. R. (1980) *J. Magn. Reson. 39*, 163.
Bystroff, C., & Kraut, J. (1991) *Biochemistry 30*, 2227.
Bystroff, C., Oatly, S. J., & Kraut, J. (1990) *Biochemistry 29*, 3263.
Cavanagh, J., Palmer, A. G., Wright, P. E., & Rance, M. (1991) *J. Magn. Reson. 91*, 429.
Cayley, P. J., Dunn, S. M. J., & King, R. W. (1981) *Biochemistry 20*, 874.
Cheng, J.-W., Lepre, C. A., & Moore, J. M. (1994) *Biochemistry 33*, 4093.
Cleland, W. W. (1975) *Acc. Chem. Res. 8*, 145.
Clore, G. M., Driscoll, P. C., Wingfield, P. T., & Gronenborn, A. M. (1990a) *Biochemistry 29*, 7387.
Clore, G. M., Szabo, A., Bax, A., Kay, L. E., Driscoll, P. C., & Gronenborn, A. M. (1990b) *J. Am. Chem. Soc. 112*, 4989.
Cowart, M., Falzone, C. J., & Benkovic, S. J. (1994) *J. Labelled Compd. Radiopharm. 34*, 67.
Creighton, T. E. (1993) *Proteins: Structures and Molecular Properties*, W. H. Freeman, New York.
Cross, T. A., & Opella, S. J. (1983) *J. Am. Chem. Soc. 105*, 306.
Falzone, C. J., Benkovic, S. J., & Wright, P. E. (1990) *Biochemistry 29*, 9667.
Falzone, C. J., Wright, P. E., & Benkovic, S. J. (1991) *Biochemistry 30*, 2184.
Falzone, C. J., Cavanagh, J., Cowart, M., Palmer, A. G., Matthews, C.R., Benkovic, S. J., & Wright, P. E. (1994a) *J. Biolmol. NMR 4*, 349.
Falzone, C. J., Wright, P. E., & Benkovic, S. J. (1994b) *Biochemistry 33*, 439.
Farnum, M. F., Magde, D., Howell, E. E., Hirai, J. T., Warren, M. S., Grimsley, J. K., & Kraut, J. (1991) *Biochemistry 30*, 11567.
Fierke, C. A., Johnson, K. A., & Benkovic, S. J. (1987) *Biochemistry 26*, 4085.
Grzesiek, S., Bax, A. (1993) *J. Am. Chem. Soc. 115*, 12593.
Gutowsky, H. S., Vold, R. L., & Wells, E. J. (1965) *J. Chem. Phys. 43*, 4107.
Herschlag, D. (1988) *Biorg. Chem. 16*, 62.
Howarth, O. W. (1978) *J. Chem. Soc., Faraday Trans. 2 74*, 1031.
Howell, E. E., Villafranca, J. E., Warren, M. S., Oatley, S. J., & Kraut, J. (1986) *Science 231*, 1123.
Jardetzky, O., & Roberts, G. C. K. (1981) *NMR in Molecular Biology*, Academic Press, New York.

Jencks, W. P. (1969) *Catalysis in Chemistry and Enzymology*, Dover, New York.
Kay, L. E., Torchia, D. A., & Bax, A. (1989) *Biochemistry 28*, 8972.
Kay, L. E., Nicholson, L. K., Delagio, F., Bax, A., & Torchia, D. A. (1992) *J. Magn. Reson. 97*, 359.
Kordel, J., Skelton, N. J., Akke, M., Palmer, A. G., & Chazin, W. J. (1992) *Biochemistry 31*, 4856.
Li, L., Falzone, C. J., Wright, P. E., & Benkovic, S. J. (1992) *Biochemistry 31*, 7826.
Lipari, G., & Szabo, A. (1982a) *J. Am. Chem. Soc. 104*, 4546.
Lipari, G., & Szabo, A. (1982b) *J. Am. Chem. Soc. 104*, 4559.
Live, D. H., Davis, D. G., Agosta, W. C., & Cowburn, D. (1984) *J. Am. Chem. Soc. 106*, 1939.
Luz, Z., & Meiboom, S. (1963) *J. Chem. Phys. 39*, 366.
Mandel, A. M., Akke, M., & Palmer, A. G. (1995) *J. Mol. Biol. 246*, 144.
Marion, D., & Wuthrich, K. (1983) *Biochem. Biophys. Res. Commun. 113*, 967.
McCammon, J. A., & Harvey, S. C. (1987) *Dynamics of Proteins and Nucleic Acids*, Cambridge University Press, Cambridge.
McConnell, H. M. (1958) *J. Chem. Phys. 28*, 430.
Meiboom, S., & Gill, D. (1958) *Rev. Sci. Instrum. 29*, 688.
Messerle, B. A., Wider, G., Otting, G. Weber, C., & Wuthrich, K. (1989) *J. Magn. Reson. 85*, 608.
Morris, G. A., & Freeman, R. (1979) *J. Am. Chem. Soc. 101*, 760.
Noggle, J. H., & Shirmer, R. E. (1971) *The Nuclear Overhauser Effect: Chemical Applications*, Academic Press, New York.
Palmer, A. G. (1993) *Curr. Opin. Biotechnol. 4*, 385.
Palmer, A. G., Rance, M., & Wright, P. E. (1991) *J. Am. Chem. Soc. 113*, 4371.
Palmer, A. G., Skelton, N. J., Chazin, W. J., Wright, P. E., & Rance, M. (1992) *Mol. Phys. 75*, 699.
Peng, J. W., & Wagner, G. (1992) *Biochemistry 31*, 8571.
Press, W. H., Flannery, B. P., Teukolsky, & Vetterling, W. T. (1986) *Numerical Recipes*, Cambridge University Press, Cambridge.
Reyes, V. M., Sawaya, M. R., Brown, K. A., & Kraut, J. (1995) *Biochemistry 34*, 2710.
Roberts, G. C. K. (1991) *Ciba Found. Symp. 158*, 169.
Shaka, A. J., Barker, P. B., & Freeman, R. (1985) *J. Magn. Reson. 64*, 547.
Skelton, N. J., Palmer, A. G., Akke, M., Kordel, J., Rance, M., & Chazin, W. J. (1993) *J. Magn. Reson., Ser. B 102*, 253.
Stone, M. J., Fairbrother, W. J., Palmer, A. G., Reizer, J., Saier, M. H., & Wright, P. E. (1992) *Biochemistry 31*, 4394.
Stone, M. J., Chandrasekhar, K., Holmgren, A., Wright, P. E., & Dyson, H. J. (1993) *Biochemistry 32*, 426.
Taylor, J. R. (1982) *An Introduction to Error Analysis*, University Science Books, Mill Valley.
Vold, R. L., Waugh, J. S., Klein, M. P., & Phelps, D. E. (1968) *J. Chem. Phys. 48*, 3831.
Wagner, C. R., & Benkovic, C. J. (1990) *Trends Biotechnol. 8*, 263.
Wagner, G., Brühwiler, D., & Wüthrich, K. (1987) *J. Mol. Biol. 196*, 227.
Wagner, G., Hyberts, S., & Peng, J. (1993) in *NMR of Proteins* (Clore, G. M., & Gronenborn, A. M., Eds.) pp 220–257, Macmillan Press, London.
Woessner, D. E. (1961) *J. Chem. Phys. 35*, 41.

BI950818A